Diffusion of small particles in a solid polymeric medium

F. Camboni, A. Koher, and I. M. Sokolov
Institut für Physik, Humboldt-Universität zu Berlin, Newtonstr. 15, D-12489 Berlin, Germany
(Received 24 October 2012; revised manuscript received 1 July 2013; published 12 August 2013)

We analyze diffusion of small particles in a solid polymeric medium taking into account a short-range particle-polymer interaction. The system is modeled by a particle diffusion on a ternary lattice where the sites occupied by polymer segments are blocked, the ones forming the hull of the chains correspond to the places at which the interaction takes place, and the rest are voids, in which the diffusion is free. In the absence of interaction the diffusion coefficient shows only a weak dependence on the polymer chain length and its behavior strongly resembles the usual site percolation. In the presence of interactions the diffusion coefficient (and especially its temperature dependence) shows a nontrivial behavior depending on the sign of interaction and on whether the voids and the hulls of the chains percolate or not. The temperature dependence may be Arrhenius-like or strongly non-Arrhenius, depending on parameters. The analytical results obtained within the effective medium approximation are in qualitative agreement with those of Monte Carlo simulations.

DOI: 10.1103/PhysRevE.88.022120 PACS number(s): 05.60.Cd, 82.35.Lr, 05.45.−a

I. INTRODUCTION

The literature treating the problem of diffusion of small molecules in solid polymeric media is surprisingly limited when compared with the huge amount of results obtained for diffusion in solids in general. This is even more surprising if one takes into account the enormous role polymeric materials play as encapsulants and isolating materials in technical devices. Diffusion of small molecules (mostly water, but also ammonia) through encapsulant layers of photovoltaic modules leads to the corrosion of the encapsulated elements and is one of the processes limiting the endurance of such appliances. The accelerated endurance tests often run at elevated temperatures and use Arrhenius law for extrapolating the results. Thus the temperature dependence of diffusion coefficient is of primary interest. This can only be understood after a general picture of small molecules' diffusion in solid polymer matrices becomes clear.

The thermodynamics of polymeric solutions and the dynamics of polymers in solutions are well understood since the seminal works by Flory [1] and Huggins [2]. The situation usually considered is the one in which polymer molecules constitute the solute of the solution. Only a few times have the roles been inverted and polymers have been taken as solvent molecules forming a matrix in which small solute particles are allowed to diffuse. Early works done in this direction observe the concentration dependence of the small solute diffusivity through experimental adsorption and desorption curves [3,4], analyze the diffusivity in the frequency domain [5], or consider both particle and polymer matrix dynamics where the latter is not assumed to be solid [6]. In particular, in [4], Fujita concludes with the necessity of theoretical and experimental investigations of the "characteristic differences"between the cases of a good or bad solubility. Up to the authors' knowledge, this request has not been satisfied yet. The aim of the present work is to give a partial answer by providing a qualitative analysis of the way the particle-phobic or particle-philic nature of the polymer chains affects the diffusion process.

In what follows we concentrate on a simple but still nontrivial conceptual model. More specifically, we consider a set of particles diffusing in an amorphous solid polymeric medium, in a model being a close relative of a classical Flory-Huggins model of polymer solutions. The dynamics of polymer chains is neglected on the time scales of interest, and the whole host system is considered as one with quenched disorder. The polymer molecules act as impenetrable obstacles for the small molecules, and the local interactions between the molecules and the polymers lead either to attraction or to repulsion between them. In the present work we adopt the ternary lattice representation corresponding to a polymer-solvent-void system close to the one proposed in Ref. [7]: in the two variants of the model considered we take a site of a lattice to represent a polymer segment, an interaction site in the vicinity of a segment, or to be empty. The concentration of solute molecules is considered low, and their interaction with each other is neglected. Finite concentrations, giving rise to nonlinear effects, could be easily included in the system, but here we want to concentrate on the simpler situation in which particles interact only with the host medium.

In the first variant of the model, polymers are represented by chains of occupied sites and their nearest neighbors are considered as interaction sites. Sites not belonging to either of these two categories are considered as voids. This lattice model is exactly the one we use in simulations. Although the model situation discussed above can be readily simulated, its analytical treatment (which may then be used for producing estimates for situations different from the ones simulated) is far from trivial even within the well-established mean-field approximation. Here, several approximations have to be done. Thus our analytical calculations refer to a simpler mean-field Flory-Huggins-like model, built by disassembling the chains and letting polymer segments, interaction, and empty sites fill the space in a completely random fashion at given concentrations. The situations are discussed in depth in Sec. II. Details of analytical calculations are given in Sec. III with a particular attention to the variations to be made with respect to the conventional effective-medium technique. In Sec. IV the interaction between the polymers and the small solute molecules is temporarily switched off and the model is reduced to a pure percolation problem in the presence of polymer chains. This is done in order to estimate the error introduced by

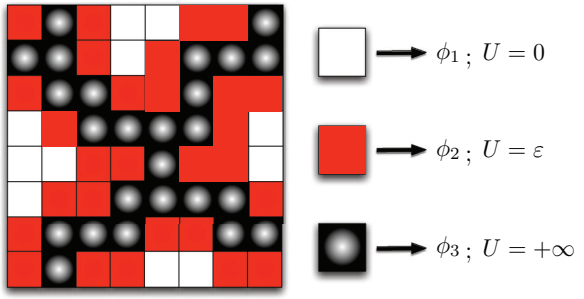

FIG. 1. (Color online) Ternary lattice of the initial model and different kinds of cells with corresponding number concentrations and energy values.

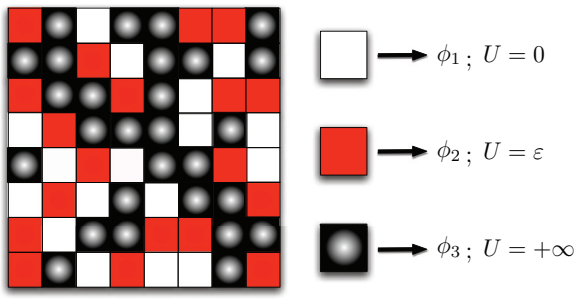

FIG. 2. (Color online) Mean-field ternary lattice and different kinds of cells with corresponding probabilities and energy values.

the mean-field approach and the dependence of the diffusion coefficient on the chain length. Section V is devoted to the role of interaction sites, and Sec. IV contains our conclusions.

II. MODEL

We model our solid polymeric matrix by a three-dimensional cubic lattice on which the chains are modeled as phantom random-walk chains of length l. This chain conformation corresponds to the Gaussian nature of chains in melts from which our solid matrix is obtained by quenching. The whole matrix is considered as static: no chain motion is taken into account. The whole system is then modeled by a ternary random potential landscape. The corresponding lattice is outlined in Fig. 1.

The sites occupied by polymer segments are impenetrable for solute molecules (hard-core interaction, interaction energy $U = \infty$) and represented as black sites in Fig. 1. The number concentration of these sites is $\phi_3 = M_3/M$, where M_3 is their total number and M is the volume (total number of sites) of the lattice.

The particle-polymer interaction is considered to take place only if the molecule occupies a site which is a nearest neighbor of the one occupied by a polymer segment. The particle-polymer interaction at these sites corresponds to the interaction energy $U = \varepsilon$ whose sign fixes the nature of the force experienced by the particles: if ε is negative, this interaction is attractive; if ε is positive, the interaction is repulsive. These interaction sites are represented in red in Fig. 1 and their number concentration is ϕ_2.

Remaining sites are considered as simple voids with energy $U = 0$ where particles perform a free motion not being subjected to any force. The number concentration of these sites is $\phi_1 = 1 - \phi_2 - \phi_3$ and they are represented in white.

Our system is thus represented by a random (but correlated) ternary lattice with the sites assigned energies U_i which take the values $0,\varepsilon$, or ∞ for the white, red, and black sites, respectively. In this medium the small molecule diffusion is numerically simulated as a nearest-neighbor random walk with transition rates between the sites given by the corresponding energy differences:

$$w_{ij} = w_0 e^{-\frac{\beta}{2}(U_i - U_j)}. \tag{1}$$

The constant rate w_0 defining the time unit of the process is set to unity in all simulations, β is the usual $1/K_BT$ term, and K_B is the Boltzmann constant. Assuming the same Arrhenius prefactors w_0 for all transitions (those within white-white, white-red, and red-red pairs) is of course a simplification which is done in order to keep the total number of parameters small. Assuming the bare rates different, i.e., introducing four different transition rates for white-white, white-red, red-white, and red-red transitions fulfilling the detailed balance condition, would of course change exact expressions for g_2 and g_3 in Eq. (7), but not the general picture of the process.

The analytical calculations are performed within a simplified model which strongly resembles the classical Flory-Huggins model ([1,2,7,8]) used for description of thermodynamical properties of polymeric solutions, in which the number concentrations of the sites occupied by polymer segments is kept, but the correlations between their positions (necessarily introduced by the existence of chains) are fully neglected. This model corresponds to filling the lattice at random with black, red, and white sites at given number concentrations. In this way each lattice site is assigned an energy value U_i which can take one of the three values $0,\varepsilon$, or ∞ at random, with probabilities ϕ_k. The existence of an infinite cluster of black sites, which we need to preserve the solidness of the system, is guaranteed by taking the concentration ϕ_3 above the percolation threshold, which is known to be approximately 0.32 for the three-dimensional simple cubic lattice. We denote this construction as mean-field lattice and represent it in Fig. 2. The diffusion on this mean-field lattice is then treated using the effective-medium approximation for a diffusion in a random potential landscape, as discussed in Sec. III. The mean-field–effective-medium results are compared with the results of direct numerical simulations discussed above, and show qualitatively similar behavior.

III. EFFECTIVE-MEDIUM APPROXIMATION FOR DIFFUSIVITY

The particles' motion in a random potential landscape is described via the usual master equation

$$\dot{q}_i = \sum_j (w_{ij} q_j - w_{ji} q_i), \tag{2}$$

where q_i is the probability for a particle to be at a site i at time t and w_{ij} is the transition rate from site j to site i given by Eq. (1) for j and i nearest neighbors and equal to

zero otherwise. For the sake of generality calculations will be referring to the d-dimensional case.

We multiply both sides of Eq. (2) by the number of particles N and obtain the master equation for the site mean number or "concentration" function $n_i = Nq_i$:

$$\dot{n}_i = \sum_j (w_{ij} n_j - w_{ji} n_i). \tag{3}$$

Assuming the existence of an equilibrium state, the transition rates are naturally linked through the detailed balance condition at equilibrium $w_{ij} n_j^0 = w_{ji} n_i^0$, where $n_i^0 = N q_i^0$ and $q_i^0 \propto \exp(-\beta U_i)$ is the equilibrium probability to find the particle at site i. Thus one can introduce the symmetrized rates g_{ij} being the properties of a bond of a lattice,

$$g_{ij} = w_{ij} n_j^0 = w_{ji} n_i^0 = g_{ji} = g_0 e^{-\frac{\beta}{2}(U_i + U_j)}, \tag{4}$$

with

$$g_0 = \frac{N w_0}{Z(\vec{\phi},\varepsilon)}, \tag{5}$$

where $Z(\vec{\phi},\varepsilon)$ is the normalization factor of q_i^0 (the partition function for the small particles equilibrium distribution) and $\vec{\phi}$ is the triplet (ϕ_1,ϕ_2,ϕ_3). Then, the analogy between the diffusion and the electric conduction in a random medium can be used [9–11]: the corresponding diffusion coefficient is connected with the macroscopic conductivity $\langle g \rangle_{em}$ of a disordered lattice with bond conductivities g_{ij} via [11–14]

$$D_{em} = a^2 \frac{\langle g \rangle_{em}}{\langle n_i^0 \rangle} = a^2 \frac{\langle w_{ji} \exp(-\beta U_i) \rangle_{em}}{\langle \exp(-\beta U_i) \rangle}, \tag{6}$$

with a the lattice spacing set to unity in all simulations. Our system exhibits four different bond conductivity values depending on the color of the sites involved. These are

$$g_1 = g_0, \quad g_2 = g_0 e^{-\beta\varepsilon}, \quad g_3 = g_0 e^{-\beta\varepsilon/2}, \quad g_4 = 0. \tag{7}$$

Figure 3 gives an overall view of this situation.

The effective conductivity $\langle g \rangle_{em}$ can then be calculated within the effective-medium approximation (EMA). There is however a subtlety in application of the effective-medium approximation to site models like ours. The genuine continuous EMA of Ref. [15] and its lattice variants Refs. [16,17] describe well the behavior of the bond percolation model but fail to reproduce the behavior for site percolation to which our ternary model reduces when $\varepsilon = 0$. For the site model, EMA procedures to obtain $\langle g \rangle_{em}$ were proposed by Bernasconi and Wiesman in [18] and Yuge in [19]: in both

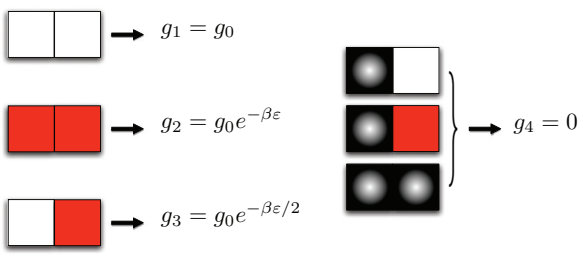

FIG. 3. (Color online) Bond conductivities for the corresponding site couples.

the usual effective-medium procedure is varied in order to take into account the correlations between consecutive bonds naturally arising in this kind of system. The fact that such correlations arise is easily understandable when considering a simple example: let us take three neighboring sites i, j, and k, where i and k are two different nearest neighbors of j, and consider the bonds ij and jk. If j is, say, white *none* of these bonds can have conductivity g_2 because both of them involve the white site j, and their conductivities are not independent as assumed in the bond-based approach, and the usual EMA technique has to be appropriately changed. Our approach here follows the lines of Ref. [19].

Calculations start by considering for any site of the lattice possessing a color index $\alpha = 1,2,3$ (corresponding to white, red, and black, respectively) the mathematical expectation of the conductivity $\bar{g}_\alpha$ of a bond starting from it:

$$\bar{g}_1 = \phi_1 g_1 + \phi_2 g_3, \quad \bar{g}_2 = \phi_1 g_3 + \phi_2 g_2, \quad \bar{g}_3 = 0. \tag{8}$$

These values appear in the system according to the probabilities of their respective sites:

$$P(\bar{g}) = \sum_{\alpha=1}^{3} \phi_\alpha \delta(\bar{g} - \bar{g}_\alpha). \tag{9}$$

The effective conductivity is then obtained through the usual self-consistency condition [16],

$$\left\langle \frac{g_{em} - \bar{g}}{(d-1)g_{em} + \bar{g}} \right\rangle_P = 0, \tag{10}$$

where d is the dimension and $\langle \cdot \rangle_P$ is the average with respect to the distribution P above. If we now define a rescaled effective conductivity,

$$f_{em} = \frac{(d-1)}{g_0} \langle g \rangle_{em}, \tag{11}$$

and introduce the arithmetic mean and the ϕ_α-weighted average of the quantity $E_i = e^{-\beta U_i/2}$,

$$\overline{E} = \tfrac{1}{3}(1 + e^{-\beta\varepsilon/2}) \quad \text{and} \quad \langle E \rangle = \phi_1 + \phi_2 e^{-\beta\varepsilon/2}, \tag{12}$$

Eq. (10) reduces to a quadratic equation for f_{em},

$$f_{em}^2 + b(\vec{\phi},\varepsilon) f_{em} + c(\vec{\phi},\varepsilon) = 0, \tag{13}$$

with

$$b(\vec{\phi},\varepsilon) = \langle E \rangle (3\overline{E} - d\langle E \rangle),$$
$$c(\vec{\phi},\varepsilon) = \langle E \rangle^2 (1 - d(1 - \phi_3)) e^{-\beta\varepsilon/2}.$$

The value of D_{em} follows from the solution of this equation via

$$D_{em} = \frac{a^2 \langle g \rangle_{em}}{\langle n_i^0 \rangle} = a^2 w_0 \frac{f_{em}}{(d-1)(\phi_1 + \phi_2 e^{-\beta\varepsilon})}$$
$$= D_0 \tilde{D}_d(\vec{\phi},\varepsilon), \tag{14}$$

where $D_0 = a^2 w_0$ is the diffusivity of a lattice where all sites are white and

$$\tilde{D}_d(\vec{\phi},\varepsilon) = \frac{f_{em}}{(d-1)(\phi_1 + \phi_2 e^{-\beta\varepsilon})} = \frac{D_{em}}{D_0} \tag{15}$$

is a normalized effective diffusivity which is due to the presence of the energy landscape.

The critical threshold at which D_{em} vanishes can be obtained by setting $c(\vec{\phi},\varepsilon) = 0$,

$$\phi_3^c = 1 - 1/d. \tag{16}$$

At variance with a classical binary Flory-Huggins situation, where the connectedness of the molecules could be disregarded to a large extent, the presence of the molecules does matter here, since it leads to a redistribution of empty sites between the red and white classes. The problem of distribution of the sites between these two classes (i.e., the one of finding ϕ_1 and ϕ_2 as functions of a given parameter ϕ_3, the polymer density) in systems with chains is a complex problem of statistical geometry, which, up to our knowledge, was never approached. We can however separate this geometrical problem (which we leave for further investigation) from the problem of the diffusion. Thus we first simulate our polymer model and extract the numerical values of ϕ_1 and ϕ_2 from these simulations. These numerical values are then used in the corresponding EMA calculations, whose predictions (for example, with respect to temperature dependence of the diffusion coefficient), in their turn, are (favorably) compared with the results of simulations of diffusion.

To get a flavor of the problem, let us first consider the situation in which the black sites are not connected into chains, but randomly distributed in the system (simple Bernoulli percolation, but now with interactions between the solute and the black matrix) on a cubic lattice with connectivity $C = 6$. This case leads to a relatively simple behavior. Black sites are randomly distributed on the lattice, and the probability that a given site is black is exactly ϕ_3; this ϕ_3 is the control parameter of the model. The site is white if it itself and none of its nearest neighbors is black, so that the concentration of the white sites is

$$\phi_1 = (1 - \phi_3)^{C+1}. \tag{17}$$

The sites which are not black or white are red, so that the concentration of red sites is

$$\phi_2 = (1 - \phi_3) - (1 - \phi_3)^{C+1}. \tag{18}$$

Thus ϕ_1 is a monotonously decaying function of ϕ_3, and ϕ_2 shows a pronounced maximum at

$$\phi_3 = 1 - \frac{1}{(C+1)^{1/C}}. \tag{19}$$

The parameter $\gamma = \phi_1/(1 - \phi_3)$, which will be repeatedly used in what follows [see Eqs. (23) and (24)], is thus given by $\gamma = (1 - \phi_3)^C$ and is a monotonously decaying function of ϕ_3.

The presence of the chains reduces the total number of available sites being neighbors of the black ones. If the molecules would follow parallel straight lines, the effective number of potentially available neighbors of black sites will be reduced to 4, so that $C = 4$ would have to be taken in the previous equation.

The numerical simulations show that the existence of the chains does matter even more. The fact that the molecules are wiggled, and the possibility of their intersection, reduces the effective values of C almost down to 2. This is made evident in Fig. 4 where the results from Eqs. (17) and (18) are plotted versus the black concentration ϕ_3 together with the values of ϕ_1 and ϕ_2 measured in simulations.

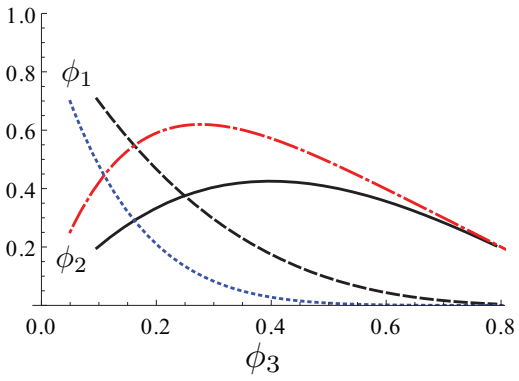

FIG. 4. (Color online) Red and white sites' concentrations in the system of chains and in the uncorrelated model. For ϕ_1 (black dashed line) and for ϕ_2 (black solid line), as well as results for uncorrelated site model: ϕ_1 as given by Eq. (17) (blue dotted line) and ϕ_2 from Eq. (18) (red dash-dotted line).

It is furthermore possible to estimate an approximate value for the effective exponent C as following from simulations. The theoretical value of the black concentration $\bar{\phi}_3$ at which white and red sites are equally distributed can be easily found by equating (17) and (18). This gives

$$\bar{\phi}_3 = 1 - \frac{1}{2^{1/C}} \quad (\simeq 0.11 \text{ for a cubic lattice}). \tag{20}$$

The simulation results in Fig. 4 lead to a larger value of $\bar{\phi}_3 \simeq 0.25$. Therefore, the value of C as obtained by inverting Eq. (20) is as low as

$$C = -\frac{\ln 2}{\ln(1 - \bar{\phi}_3)} \simeq 2.41. \tag{21}$$

IV. PURE PERCOLATION (BINARY) MODEL

It would be nice to know how large is the typical error arising from disregarding the chain structure of black sites, and what is the role the chain length plays in the simplest case, namely in a percolation model with correlated black sites given by the chains. In this model the red and the white sites are indistinguishable; they have the total number concentration $\phi_1 = 1 - \phi_3$, and the result of our previous consideration reduces to the original Yuge's result for site percolation. This is exactly the situation discussed in the present section.

Thus we consider a pure percolation situation in which the only interactions are the excluded volume ones and our lattice consists of only black and white sites; red ones are absent. The results of simulations for the systems of chains of different lengths are shown in Fig. 5(a). The figure representing the dependence of the diffusion coefficient on the concentration of sites occupied by segments of the chain shows this for the chain lengths from $l = 1$ (usual Bernoulli site percolation problem) to $l = 10$. The simulations were performed also for longer chains, but for l larger than 10 the corresponding graphs are indistinguishable from that for $l = 10$ within the statistical accuracy. Thus a result for $l = 100$ (not shown) is indistinguishable from the one for $l = 10$ on the scales of Fig. 5(a).

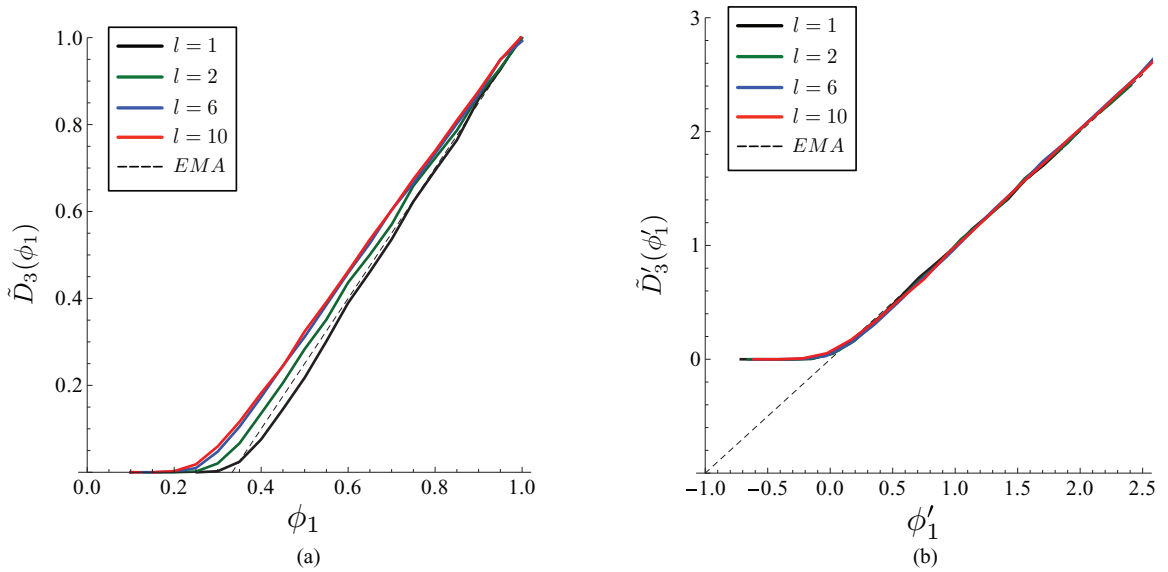

FIG. 5. (Color online) (a) Normalized diffusivities $\tilde{D}_3$ in the purely percolation case vs the concentration ϕ_1 of white sites; (b) rescaled normalized diffusivities $\tilde{D}'_3$ vs rescaled white concentration ϕ'_1. The dotted line represents in both figures the effective medium approximation.

Details about simulations are readily given: simple random walks of l steps are let run independently in a lattice of 400^3 sites with periodic boundary conditions. This operation is stopped when the total concentration of segments (sites visited at least once) is within 0.01 from the desired value of ϕ_3. Once the environment is created, 10^6 random walks of 10^3 to 10^4 steps, depending on the speed of homogenization of the system, are launched from a free site chosen at random in a cube of 50^3 sites placed in the center of the medium. With this choice, the probability for a diffusing particle to reach the borders of the lattice is extremely low and doesn't spoil the statistics. The algorithm used is the Monte Carlo Blind Ant one. The whole procedure is then repeated for 10 different lattice realizations and averages are taken. We have observed a normal diffusion process $\langle r^2(t)\rangle \propto t$ from which the proportionality constant $\tilde{D}_3$ has been extracted and reported in Fig. 5(a). The homogenization of $\langle r^2(t)\rangle$ slows down in the proximity of the critical point. For this reason 10^4 time steps become insufficient and the diffusivity is systematically overestimated. Our attention, however, is focused on a range of values of ϕ_3 which are above the percolation threshold.

The curves do not differ drastically, but definitely show different percolation thresholds $\phi_1^c(l)$ depending on l. For the Bernoulli case the total behavior of diffusivity is reproduced sufficiently well by EMA for ϕ_3 close to unity but departs from the EMA line for concentrations close to a critical one. For longer chains the critical concentration gets lower, and the diffusion coefficient at given ϕ_1 gets larger than for the Bernoulli case. Although different, the curves, however, show a large amount of universality which is unveiled when rescaling the concentration and diffusivity according to

$$\phi'_1 = \frac{\phi_1}{\phi_1^c} - 1 \quad \text{and} \quad \tilde{D}'_3 = \tilde{D}_3 \frac{\left(1-\phi_1^c\right)}{\phi_1^c}, \tag{22}$$

so that the critical concentration is mapped onto the point $\phi'_1 = 0$; see Fig. 5(b). In this case all the curves fall onto the same master curve, and the mean-field result, rescaled accordingly, gives a straight line (of slope 1) which reproduces the results of simulations astonishingly well up to the critical domain. This high degree of universality shows that the correlations introduced by the existence of the chains are not of high importance and can be fully accounted for by rescaling the results of EMA according to the equations above. The corresponding critical concentration has, however, to be obtained numerically. Alternatively, it can be extrapolated from the slope of diffusion coefficient for concentrations close to unity.

V. RESULTS FOR TERNARY MODEL

In this section we discuss results for the normalized effective diffusivity $\tilde{D}_3(\vec{\phi},\varepsilon)$ and concentrate on the role of interaction energy ε between the diffusing particles and the polymer matrix. All the figures refer to the three-dimensional case. The reduced interaction energy $\beta\varepsilon = \bar{\varepsilon}$ is chosen to span in the interval $[-5,5]$ according to the following reasoning: typical absolute values of ε_{XX}/K_B, the coupling strength of a Lennard-Jones potential describing the interaction between two atoms of the same kind X, can be roughly enclosed in the interval corresponding to temperatures [0,500 K] [20–22]. In order to consider the interaction between two different atoms X and Y, the Lorentz-Berthelot mixing rule is used to obtain $\varepsilon_{XY} = \sqrt{\varepsilon_{XX}\varepsilon_{YY}}$ which, being an average, belongs to the same interval. Using ε in place of ε_{XY}, considering both positive and negative values and taking the temperature not too far from the ambient one, it is straightforward to see that the choice $\bar{\varepsilon} \in [-5,5]$ is a reasonable one. For the discussion of the Arrhenius or non-Arrhenius temperature dependencies in Sec. V B broader bounds are used: $\bar{\varepsilon} \in [-10,10]$.

A. Effective diffusivity vs interaction energy

Let us first discuss general features of the dependence of the diffusion coefficient on number concentrations and on interaction energy ε. The EMA results for $\tilde{D}_3(\vec{\phi},\varepsilon)$ in

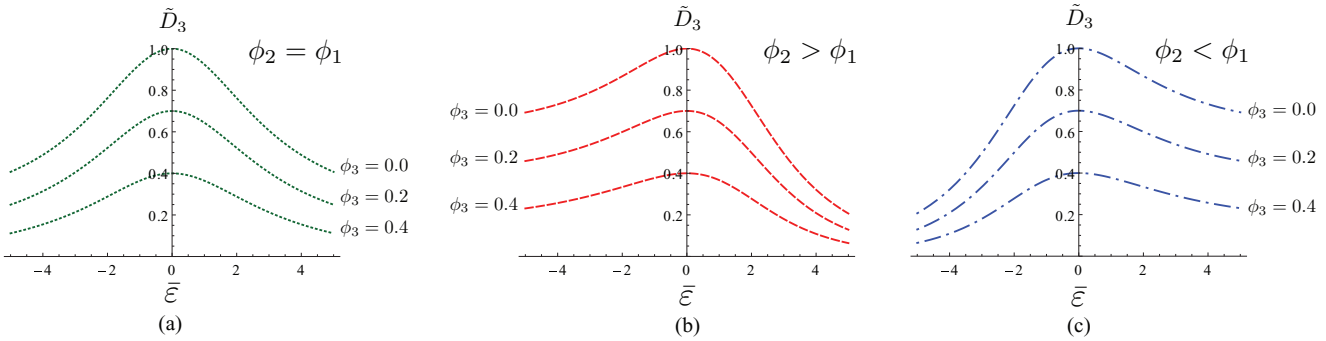

FIG. 6. (Color online) EMA normalized effective diffusivity $\tilde{D}_3$ vs $\bar{\varepsilon}$ in the cases $\phi_3 = 0$, 0.2, and 0.4 and (a) $\gamma = 1/2$, (b) $\gamma = 1/4$, and (c) $\gamma = 3/4$.

the three different cases corresponding to different relations between ϕ_1 and ϕ_2 at ϕ_3 fixed are shown in Fig. 6. These plots show the behavior for the attractive and repulsive interaction and the way the diffusivity approaches zero when the black sites concentration approaches its critical value $\phi_3^c = 2/3$ [see Eq. (16)]. At this value, in fact, particles remain confined in finite subregions of the system, due to the overwhelming predominance of polymer segments.

Plots are given for three different sets of the ϕ_k values in order to consider symmetrically the situations in which red sites are in minority, equally probable, or predominant with respect to the white ones, at given ϕ_3. For this purpose we introduce the real parameter $\gamma \in [0,1]$ we previously mentioned, and define the number concentrations of white and red sites as

$$\phi_1 = \gamma(1 - \phi_3), \tag{23}$$

$$\phi_2 = (1 - \gamma)(1 - \phi_3). \tag{24}$$

Graphs are then taken for three different values of γ (color online): $\gamma = 1/4$ (red dashed lines, $\phi_2 > \phi_1$), $\gamma = 1/2$ (green dotted lines, $\phi_2 = \phi_1$), and $\gamma = 3/4$ (blue dash-dotted lines, $\phi_2 < \phi_1$).

This imbalance will deeply influence the behavior of the effective diffusivity when ε crosses the zero value. In the symmetric case $\phi_2 = \phi_1$, $\tilde{D}_3$ is invariant under the change of the sign of interaction energy $\bar{\varepsilon} \to -\bar{\varepsilon}$. On the contrary, when the white-red balance is broken, the effective diffusivity decreases or increases depending on the sign of the energy parameter and on the value of γ.

To better explain, let us consider the situation in which $\phi_2 > \phi_1$ [e.g., $\gamma = 1/4$, Fig. 6(b), red solid lines] and restrict our attention to the attractive $\bar{\varepsilon} < 0$ region; with this choice of the parameters, we have increased the number of the red-red g_2 bonds (showing larger conductivity) with respect to the number of the white-white g_0 ones which have the lowest conductivity. This results in a global increasing of the effective diffusion constant. If we now invert the sign of ε, i.e., consider the repulsive interaction, the g_2 bonds are still the most numerous, but now they bring the lowest conductivity value, decreasing in this way the whole diffusivity of the system. The opposite happens if we consider $\phi_2 < \phi_1$ and the corresponding graph in Fig. 6(c) results in a mirror image of the one in Fig. 6(b).

The comparison between the mean-field calculations and the Monte Carlo simulations performed in the original ternary lattice with the chain length $l = 100$ is quite satisfactory (Fig. 7). Once the desired polymer concentration was reached and the polymer matrix is set up, the energy value ε is assigned to all the nearest neighbors of the segments and their concentration ϕ_2 is measured. All results are averaged over 10 realizations of the polymeric matrix. In each of them 10^6 random walks of 10^4 steps are performed as described above.

Representative samples corresponding to the cases $\phi_2 > \phi_1$, $\phi_2 \simeq \phi_1$, and $\phi_2 < \phi_1$, namely, the red, green, and blue ones, were found according to the suggestions of Fig. 4, giving the concentration values reported in Fig. 7. The numerical

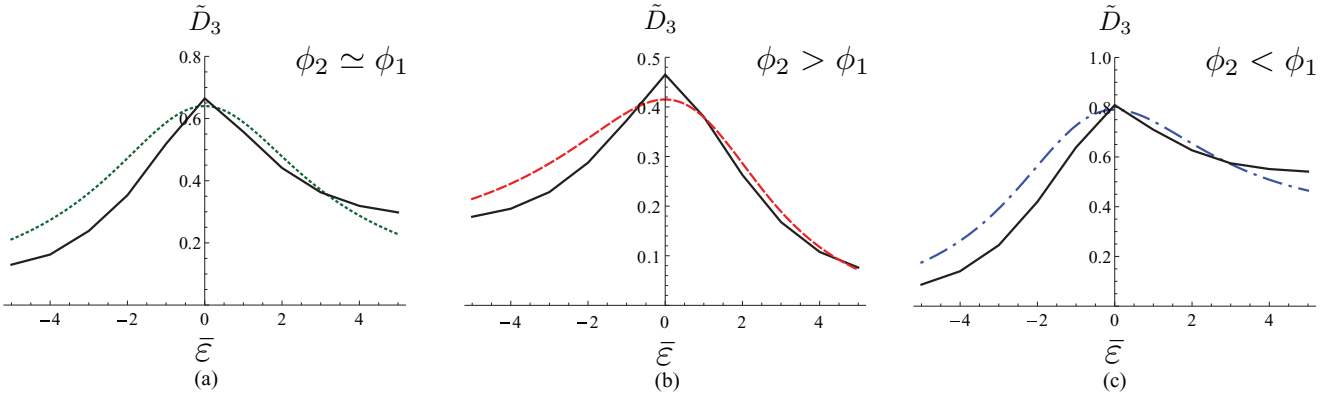

FIG. 7. (Color online) Comparison between theory and simulations (black solid line) in the following cases: (a) $\phi_1 = 0.39$, $\phi_2 = 0.37$, $\phi_3 = 0.24$ ($\gamma = 0.513\,158$); (b) $\phi_1 = 0.18$, $\phi_2 = 0.43$, $\phi_3 = 0.39$ ($\gamma = 0.295\,082$); (c) $\phi_1 = 0.59$, $\phi_2 = 0.27$, $\phi_3 = 0.14$ ($\gamma = 0.686\,047$).

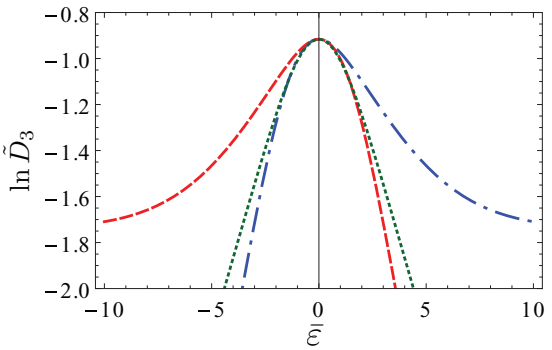

FIG. 8. (Color online) Arrhenius plots of the different EMA normalized effective diffusivities vs $\bar{\varepsilon}$ at $\phi_3 = 0.4$ and $\gamma = 1/4$ (red dashed line), $\gamma = 1/2$ (green dotted line), and $\gamma = 3/4$ (blue dash-dotted line).

result is plotted together with the mean-field calculations in which the same values are used. We note that the value of the polymer concentration is close to the critical domain in Fig. 7(b) corresponding to $\varepsilon = 0$, so that the total accuracy of EMA is not too high in this domain. However, the EMA results reproduce the dependence qualitatively well and, moreover, the accuracy of EMA improves for higher interaction strengths.

B. Arrhenius vs non-Arrhenius behavior

A nontrivial aspect of the dependence of diffusivity on the interaction strength is revealed by the Arrhenius plots shown in Fig. 8 where the logarithm of $\tilde{D}_3$ is plotted as a function of $\bar{\varepsilon} = \varepsilon/K_BT$ in the wider interval $[-10,10]$ to investigate the role played by activation in the diffusion process; the segment concentration is set here to $\phi_3 = 0.4$. The three curves correspond to the values of $\gamma = 1/4$ (red dashed line), $\gamma = 1/2$ (green dotted line), and $\gamma = 3/4$ (blue dash-dotted line). As in the previous figures, the curve for $\gamma = 1/2$ represents an even function of $\bar{\varepsilon}$, and the curves for $\gamma = 1/4$ and $\gamma = 3/4$ are mirror images of each other. For $\bar{\varepsilon}$ close to zero, the activation process is not relevant, the curves fall together and reproduce the diffusion constant in the black-and-white lattice of Sec. IV. When moving away from the $\bar{\varepsilon} = 0$ value, the activation acquires importance. For $\gamma = 1/2$ this behavior becomes Arrhenius-like and the curve shows a linear decay for both signs of $\bar{\varepsilon}$ provided the interaction is strong enough. For asymmetric cases $\gamma \neq 1/2$ the Arrhenius behavior is seen only for interaction energy of the corresponding sign (attractive interaction for $\gamma < 1/2$ and repulsive interaction for $\gamma > 1/2$). For the opposite sign of interaction, at low temperatures, or high absolute values of ε, the lines become horizontal, quitting the Arrhenius regime.

This non-Arrhenius behavior can be explained as follows. Let us focus our attention again on the red (dashed) line in the negative $\bar{\varepsilon}$ half-plane. Under segment concentration $\phi_3 = 0.4$ the black infinite cluster exists but is not dense enough to prevent the existence of infinite white or red ones. The concentration of red sites is $\phi_2 = 0.45$ ($\gamma = 1/4$) and thus lays above the percolation threshold for a cubic lattice. This means that red sites form an infinite cluster crossing the whole system, and once a particle finds it, it becomes more probable to travel along it than escape from it by activation. As a consequence diffusivity saturates and the system never freezes. In the repulsive region, the same behavior is shown by the blue (dash-dotted) line, indicating the existence of a white infinite cluster.

The green (dotted) line, the one for symmetric situation $\phi_3 = 0.4$, $\phi_2 = \phi_1 = 0.3$, doesn't show any saturation. This suggests that in such a case white and red concentrations are below the percolation threshold, and the activation processes are necessary to traverse the system.

Figure 9 shows the comparison between theory and simulation Arrhenius plots in the original interval $\bar{\varepsilon} \in [-5,5]$ and for the same concentration values of Fig. 7.

On the total the following regimes of behavior can be qualitatively distinguished.

(1) If the concentration of black sites is so high that percolation on red and white sites is not possible, the diffusion coefficient vanishes.

In the case when percolation over the red-and-white domains is possible, the diffusion coefficient is nonzero, and its behavior as a function of temperature depends on the percolation properties of red and white clusters, and on the sign of interaction energy.

If the interaction is repulsive, two regimes appear as follows.

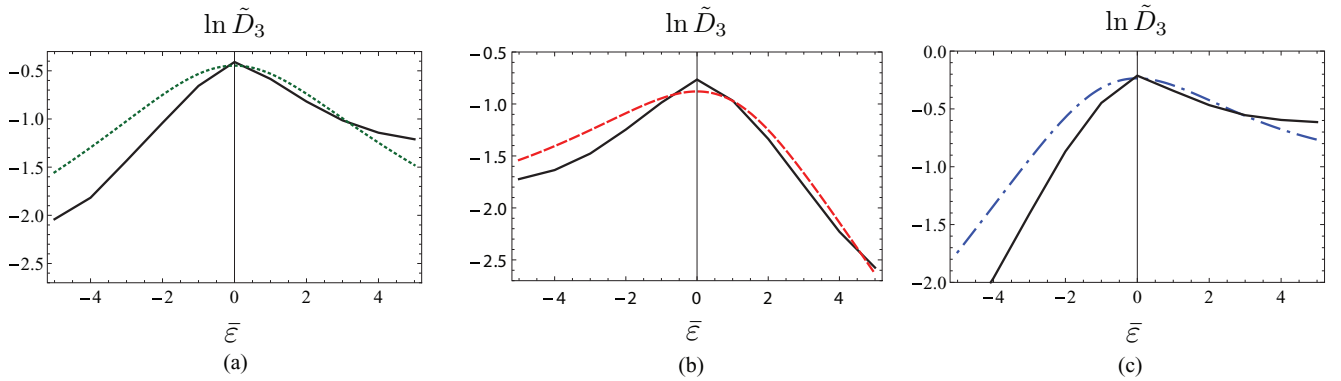

FIG. 9. (Color online) Comparison between theory and simulation (black solid lines) Arrhenius plots at (a) $\phi_1 = 0.39$, $\phi_2 = 0.37$, $\phi_3 = 0.24$ ($\gamma = 0.513\,158$, $\phi_2 \simeq \phi_1$), (b) $\phi_1 = 0.18, \phi_2 = 0.43, \phi_3 = 0.39$ ($\gamma = 0.295\,082$, $\phi_2 > \phi_1$), and (c) $\phi_1 = 0.59, \phi_2 = 0.27, \phi_3 = 0.14$ ($\gamma = 0.686\,047$, $\phi_2 < \phi_1$).

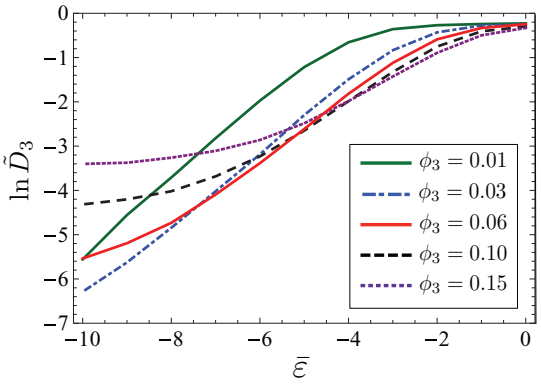

FIG. 10. (Color online) Simulation graph: Arrhenius plots of the normalized diffusivity in the attractive case vs $\bar{\varepsilon}$ for different segment concentrations.

(2) If white sites percolate, the diffusion over the white cluster is always possible and does not need activation. The temperature dependence saturates.

(3) If white clusters do not percolate, the diffusion is only possible over red sites, and involves an activation process; its temperature dependence shows the Arrhenius behavior.

In the case of attractive interaction the roles of white and red sites interchange, and percolation over red sites is what determines the temperature dependence of the diffusion coefficient as follows.

(4) If red sites do percolate, the diffusion over the red cluster is possible and does not need activation. The temperature dependence saturates.

(5) If red clusters do not percolate, the diffusion has to go via white sites, and therefore involves an activation process; its temperature dependence shows the Arrhenius behavior.

These features, predicted by EMA, have also been found in simulations of a genuine ternary lattice in which red clusters run clung on the black chains by construction. Figure 10 shows the behavior of Arrhenius plots for low polymer concentrations in the case of attractive interaction. It shows the logarithm of the normalized effective diffusivity for different values of ϕ_3. For $\phi_3 < 0.06$, polymers remain sparse and isolated, their red perimeter sites don't percolate, no infinite red cluster exists, and the system is in an Arrhenius regime (5). When the number of chains is increased, the transition from the Arrhenius to the saturation behavior (4) is observed at the critical value $\phi_3 = 0.06$, revealing the emergence of an infinite red cluster. This critical value is far below the usual percolation threshold of a cubic lattice due to the fact that red sites are arranged in connected groups on the perimeters of black chains. This number cannot be predicted by simple EMA and can be translated into an estimate of the percolation threshold of perimeter sites of chains.

VI. CONCLUSIONS

We have considered diffusion of small molecules in a solid polymeric medium taking into account the interaction between polymers and diffusing particles which can be both attractive or repulsive. The diffusivity has been analyzed from different perspectives both analytically, using a modified effective-medium approximation, and numerically by performing direct Monte Carlo simulations. While the diffusivity is only slightly affected by the chain's length, its temperature dependence crucially depends on the kind of interaction. This behavior depends on the sign of the interaction energy and is related to the existence of a percolating cluster of interaction sites surrounding polymer segments and/or a percolating cluster of voids on which particles are free to travel without activation.

ACKNOWLEDGMENT

The work was supported by BMU within the project "Zuverlässigkeit von PV Modulen II."

[1] P. J. Flory, J. Chem. Phys. **10**, 51 (1942).
[2] M. L. Huggins, J. Phys. Chem. **46**, 151 (1942).
[3] A. Kishimoto, E. Maekawa, and H. Fujita, Bull. Chem. Soc. Jpn. **33**, 988 (1960).
[4] H. Fujita, Fortschr. Hochpolym. Forsch. **3**, 1 (1961).
[5] B. M. Schulz, A. Karatchentsev, M. Schulz, and W. Dieterich, J. Non-Cryst. Solids **352**, 5136 (2006).
[6] O. Dürr, W. Dieterich, and A. Nitzan, J. Chem. Phys. **121**, 12732 (2004).
[7] M. G. Bawendi and K. F. Freed, J. Chem. Phys. **88**, 2741 (1988).
[8] M. G. Bawendi, K. F. Freed, and U. Mohanty, J. Chem. Phys. **84**, 7036 (1986).
[9] J. P. Bouchaud and A. Georges, Phys. Rep. **195**, 127 (1990).
[10] P. G. Doyle and J. L. Snell, *Random Walks and Electrical Networks* (The Mathematical Association of America, Washington, DC, 1984).
[11] F. Camboni and I. M. Sokolov, Phys. Rev. E **85**, 050104(R) (2012).
[12] D. S. Dean, I. T. Drummond, and R. R. Horgan, J. Stat. Mech. (2007) P07013.
[13] P. Maass, B. Rinn, and W. Schirmacher, Phil. Mag. B **79**, 1915 (1999).
[14] B. Rinn, U. Braunschweig, P. Maass, and W. Schirmacher, Phys. Status Solidi B **218**, 93 (2000).
[15] D. A. G. Bruggeman, Ann. Phys. **24**, 636 (1935).
[16] S. Kirkpatrick, Rev. Mod. Phys. **45**, 574 (1973).
[17] J. W. Haus and K. W. Kehr, Phys. Rep. **150**, 263 (1987).
[18] J. Bernasconi and H. J. Wiesman, Phys. Rev. B **13**, 1131 (1976).
[19] Y. Yuge, J. Stat. Phys. **16**, 339 (1977).
[20] N. M. Putintsev and D. N. Putintsev, Dokl. Phys. Chem. **399**, 278 (2004).
[21] N. Bernardes, Phys. Rev. **112**, 1534 (1958).
[22] C. Kittel, *Introduction to Solid State Physics* (Wiley, New York, 1974).